

Remarkable thermoelectric performance in BaPdS₂ via pudding-mold band structure and ultralow lattice thermal conductivity

Eric B. Isaacs and Chris Wolverton*
*Department of Materials Science and Engineering,
 Northwestern University, Evanston, Illinois 60208, USA*
 (Dated: July 28, 2021)

Efficient thermoelectric materials require a rare and contraindicated combination of materials properties: large electrical conductivity, large Seebeck coefficient, and low thermal conductivity. One strategy to achieve the first two properties is via low-energy electronic bands containing both flat and dispersive parts in different regions of crystal momentum space, known as a pudding-mold band structure. Here, we illustrate that BaPdS₂ successfully achieves the pudding-mold band structure, contributing to a large thermoelectric power factor, due to its anisotropic crystal structure containing zig-zag chains of edge-sharing square planar PdS₄ units. In addition, BaPdS₂ exhibits ultralow lattice thermal conductivity, and thus also achieves the third property, due to extremely soft and anharmonic interactions in its transverse acoustic phonon branch. We predict a remarkably large thermoelectric figure of merit, with peak values between 2 and 3 for two of the three crystallographic directions, suggesting BaPdS₂ warrants experimental investigation.

I. INTRODUCTION

The figure of merit for a thermoelectric material, which can convert a temperature gradient into electrical current, is

$$ZT = \frac{S^2 \sigma}{\kappa_{el} + \kappa_L} T, \quad (1)$$

where S , σ , T , κ_{el} , and κ_L are the Seebeck coefficient, electrical conductivity, temperature, electrical contribution to thermal conductivity, and lattice contribution to thermal conductivity, respectively.^{1,2} One strategy to achieve a large ZT is via engineering the electronic band structure, i.e., the electron energy ε as a function of crystal momentum \mathbf{k} .³ In particular, a band with both flat (small $\nabla_{\mathbf{k}}\varepsilon$) and dispersive (large $\nabla_{\mathbf{k}}\varepsilon$) parts along a direction in \mathbf{k} -space has been shown to enhance σS^2 if the electron chemical potential μ lies at an energy separating the two regions.⁴ In such a “pudding-mold” band structure, the band velocity difference leads to large S , and large σ is achieved due to the dispersive part of the band and a large Fermi surface.⁴ More generally, one can consider a broader definition of a pudding-mold band structure in which the flat and dispersive regions can along different directions in \mathbf{k} -space, which naturally occurs for low-dimensional bulk and nanostructured crystals.^{5–7} The pudding-mold band structure has been used to explain the promising thermoelectric performance of Na_xCoO₂,⁴ SnSe,^{8–10} and recently-proposed Fe-based Heusler compounds¹¹ among others.

Recently, the promising thermoelectric performance of several Pd oxide compounds has been attributed in part to the pudding-mold band structure. The layered compound PbPdO₂, for example, exhibits a large Seebeck coefficient of 175 $\mu\text{V}/\text{K}$ at 600 K when hole doped.¹² Based on first-principles calculations, hole-doped Bi₂PdO₄ was predicted to exhibit high power factor (σS^2) in addition to low κ_L .¹³ In both of these compounds, achieving the pudding-mold band structure appears to be connected

to the presence of square planar Pd²⁺. Based on this observation, we previously developed an inverse band structure design approach based on a materials database screening to search for other square planar compounds achieving the pudding-mold band structure.¹⁴ Although several chemistries were considered, we focused on oxide materials such as Ba₂PdO₃ and La₄PdO₇ in order to validate the approach.

The thermoelectric efficiency of oxides is often limited by (1) large κ_L , stemming from the low atomic mass of oxygen and rigid chemical bonding, and (2) low carrier mobility.^{15,16} Therefore, in this work, we turn our attention to *chalcogenide* materials. Chalcogenides comprise many of the most-investigated and highest-performance thermoelectrics, such as PbTe, Bi₂Te₃, SnSe, Cu₂(S/Se), and La_{3–x}Te₄.^{17–19} We investigate a chalcogenide material based on square planar Pd, namely BaPdS₂, with the aim of achieving low κ_L in addition to pudding-mold band structure. BaPdS₂ is the only such square planar chalcogenide identified by our previous inverse band structure design approach¹⁴ other than metallic EuPd₃S₄²⁰ and the binaries PdS₂²¹ and PdSe₂.²² Although BaPdS₂ was first synthesized in 1986,²³ it has not been explored as a thermoelectric material to the best of our knowledge. The presence of heavy Ba, in addition to the lack of oxygen, leads to the potential for low κ_L . Using electronic structure and transport calculations based on the density functional theory, we find that BaPdS₂ exhibits (1) a pudding-mold band structure for p -type doping, (2) large power factor for both n - and p -type doping, (3) ultralow κ_L due to extremely soft and anharmonic bonding, and (4) highly-anisotropic electronic and thermal transport behavior. We find remarkable predicted thermoelectric performance, with ZT larger than 2 in certain crystallographic directions at high temperature, assuming optimal doping and using a reasonable value of electronic relaxation time τ (5 fs).^{11,24–28} Based on these results, we suggest BaPdS₂ warrants experimental investigation.

II. COMPUTATIONAL DETAILS

We perform density functional theory^{29,30} calculations using the generalized gradient approximation³¹ and the projector augmented wave method (Ba,sv, Pd, and S potentials)^{32,33} in the Vienna *ab initio* simulation package (VASP).^{34–37} A plane wave basis with 500 eV kinetic energy cutoff and uniform k -meshes with ≥ 700 k -points per \AA^{-3} are employed. The ionic forces and total energy are converged to 10^{-3} eV/ \AA and 10^{-6} eV, respectively. High-symmetry k - and q -point paths are based on the conventions of Setyawan *et al.*³⁸

Semiclassical electronic transport calculations within the constant relaxation time (τ) approximation are performed using BOLTZTRAP³⁹ with k -point density of $3,500/\text{\AA}^{-3}$. Phonon calculations are performed using the direct approach in PHONOPY⁴⁰ with a 192-atom supercell chosen to be approximately cubic based on the algorithm of Erhart *et al.*⁴¹ as implemented in ASE.⁴² The mode Grüneisen parameter is computed using a $\pm 0.3\%$ volume difference. κ_L is computed via the Debye-Callaway model^{43–45} and compared to that of the minimum thermal conductivity model of Cahill *et al.*⁴⁶ κ_{el} is computed via the Wiedemann-Franz law. Additional details on the electronic and thermal transport calculations are included in the Supplemental Material.⁴⁷

III. RESULTS AND DISCUSSION

BaPdS₂, shown in Fig. 1(a) and Fig. 1(b), has a C-centered orthorhombic unit cell with space group $Cmcm$. Isostructural to BaNiO₂, it consists of 1D chains of edge-sharing PdS₄ square planar units (corresponding to a PdS₂ composition) connected in a zig-zag pattern. The computed lattice parameters, atomic positions, and formation energy are in good agreement with experimental values, as discussed in the Supplemental Material. The electronic band structure of BaPdS₂ is shown in Fig. 1(c). The valence band, which consists primarily of Pd d states, exhibits a pudding-mold band structure. It is dispersive in the direction along the 1D chains (e.g., Γ -Z) and flat along other directions (e.g., Γ -X and Γ -Y). In other words, the pudding-mold band structure is closely related to the highly-anisotropic crystal structure of BaPdS₂. We do not find a pudding-mold band structure for the conduction band, which consists of a hybridization of Pd d and S p orbitals. We note that an additional conduction band minimum between S and R is close in energy (~ 130 meV) to the band edge at Γ .

The band structure of BaPdS₂ leads to notable electronic transport properties. Figure 2(a) illustrates the behavior of the average (over Cartesian directions) of $\sigma S^2/\tau$ as a function of carrier concentration for several temperatures. Results for BaPdS₂ are shown in comparison to those of SnSe, a high-performing thermoelectric material.^{8,48–50} BaPdS₂ achieves comparable p -type power factor behavior to SnSe, albeit at larger (though

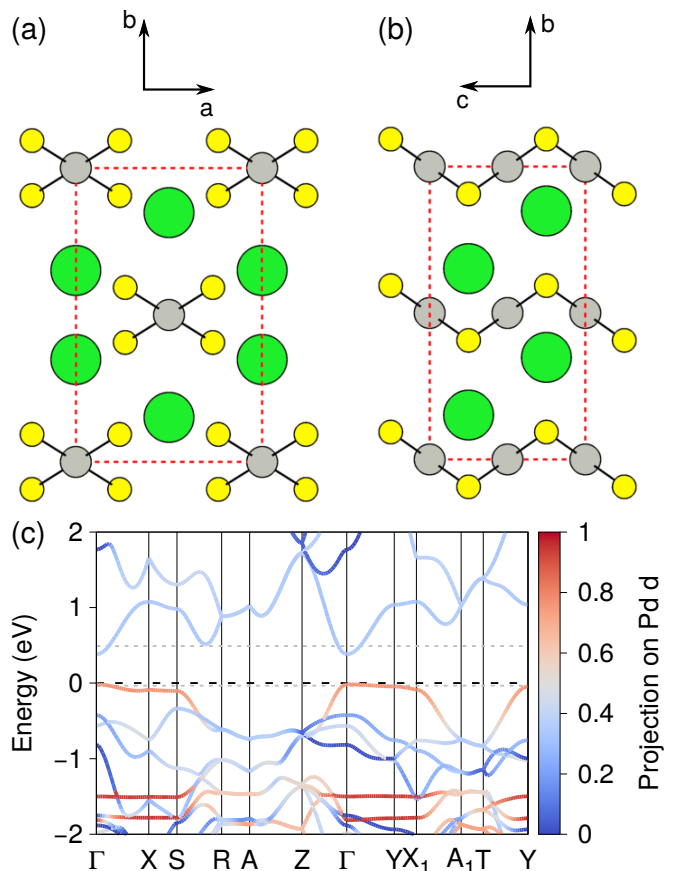


FIG. 1. Orthographic projection of the crystal structure of BaPdS₂ along the (a) c and (b) a axes of the conventional unit cell (red dashed lines). The green, gray, and yellow circles represent Ba, Pd, and S atoms, respectively. Black lines indicate the Pd-S bonds of the square planar units. (c) The electronic bands of BaPdS₂ colored by the Pd d character of the electronic states. The black dashed line corresponds to the valence band minimum, and the gray horizontal dotted lines indicate the $\pm 10^{20}$ cm^{-3} doping levels.

still reasonable¹⁷) doping values. For example, at 700 K, the maximum predicted p -type $\sigma S^2/\tau$ is $\sim 3 \times 10^{11}$ W/(m·K²·s) for both BaPdS₂ (for 7×10^{20} holes/cm³) and SnSe (for 3×10^{20} holes/cm³). We also note that the p -type power factor behavior exhibits significantly less temperature dependence for BaPdS₂ than for SnSe. Although the conduction band does not exhibit pudding-mold qualities, we find even larger $\sigma S^2/\tau$ for n -type doping, though smaller than the corresponding SnSe behavior. For example, the peak n -type $\sigma S^2/\tau$ for BaPdS₂ at 700 K is 5.3×10^{11} W/(m·K²·s), occurring at a doping value of $\sim 5.5 \times 10^{20}$ electrons/cm³; SnSe exhibits a significantly larger peak n -type $\sigma S^2/\tau$ of 8.4×10^{11} W/(m·K²·s) at around the same doping magnitude. The appreciable n -type power factor behavior for BaPdS₂ likely stems from the band convergence,^{51–55} i.e., the small energy separation between the conduction band minima (1) at Γ and (2) between S and R.

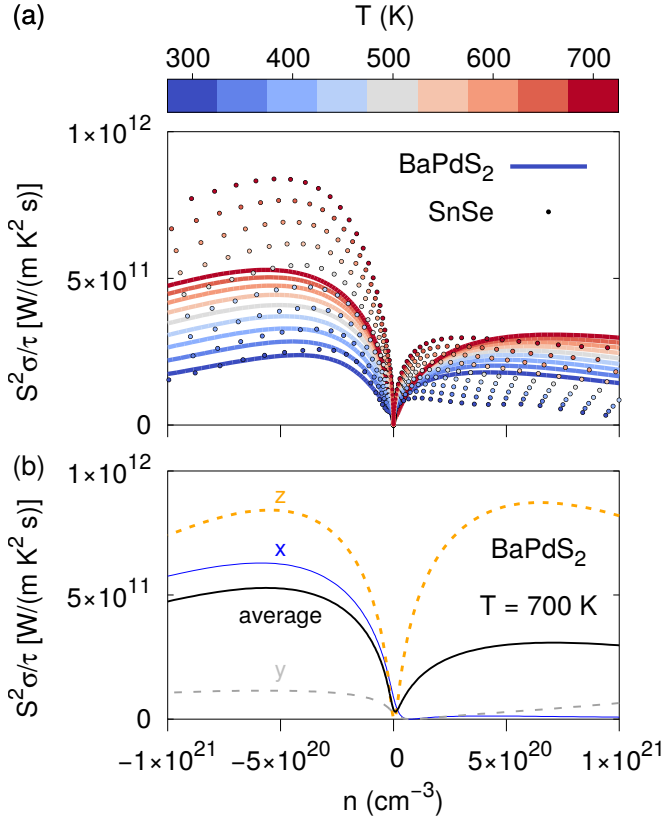


FIG. 2. (a) Power factor divided by electronic relaxation time as a function of carrier concentration for BaPdS₂ (lines) and SnSe (circles), averaged over the x , y , and z directions, for several values of T . (b) $T = 700$ K power factor divided by electronic relaxation time versus carrier concentration in each direction, in addition to the average, for BaPdS₂.

Due to the structural anisotropy, the power factor behavior for BaPdS₂ is highly anisotropic. We illustrate the power factor behavior at 700 K, for example, in Fig. 2(b) for each direction. For hole doping, $\sigma S^2/\tau$ is only appreciable along the z direction (i.e., along the 1D chains), which is consistent with the pudding-mold band structure. In contrast, for electron doping, large $\sigma S^2/\tau$ is observed in both the z and x directions. A rationalization for the lower n -type power factor behavior in the y direction is discussed in the Supporting Information.

Branch	v_x	v_y	v_z	$\Theta_{\Gamma X}$	$\Theta_{\Gamma Y}$	$\Theta_{\Gamma Z}$
TA	0.5	1.9	0.8	43	49	42
TA'	2.4	2.4	1.9	82	54	72
LA	4.1	3.7	3.6	99	115	72

TABLE I. Group velocity v at Γ (in km/s) and Debye temperature Θ (in K) of BaPdS₂ for each acoustic branch and direction.

Having established the promising predicted electronic transport properties of BaPdS₂, we now turn our at-

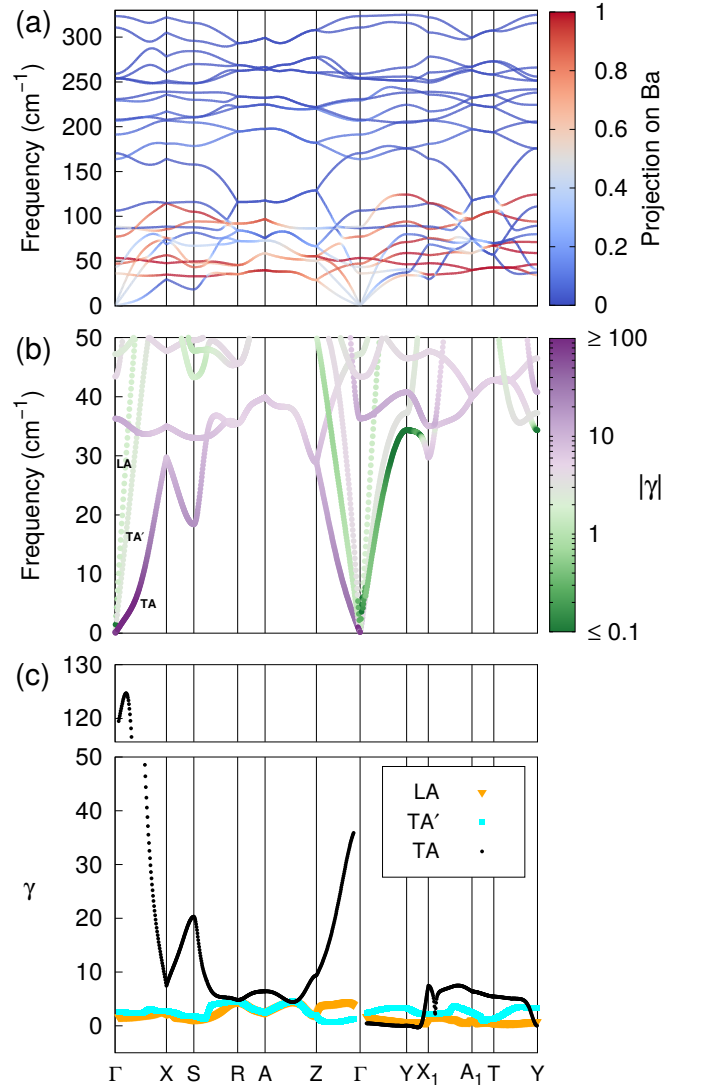


FIG. 3. (a) BaPdS₂ phonon bands colored by Ba contribution to the phonon eigenvector. (b) The low-frequency portion of the phonon dispersion with bands colored by the magnitude of the mode Grüneisen parameter. (c) Dispersion of the mode Grüneisen parameter $\gamma_{\mathbf{q}\nu}$ for the acoustic branches. Due to the large $\gamma_{\mathbf{q}\nu}$ values for the TA branch along Γ -X, we use a broken $\gamma_{\mathbf{q}\nu}$ axis for clarity.

tention to thermal transport. The phonon dispersion of BaPdS₂ is shown in Fig. 3(a). Low-frequency optical modes, primarily involving vibration of the heavy Ba atoms, are observed in the ~ 30 – 110 cm⁻¹ frequency range. For each acoustic branch, we compute the group velocity in the long-wavelength limit (v_x , v_y , and v_z) and Debye temperature ($\Theta_{\Gamma X}$, $\Theta_{\Gamma Y}$, and $\Theta_{\Gamma Z}$) for each direction, as shown in Table I. Here, we define Θ as the acoustic phonon frequency at the zone boundary, and the acoustic branch definitions are given in the Supplemental Material. BaPdS₂ is a very soft material, exhibiting low group velocities (0.5–4.1 km/s) and Debye tempera-

tures (42–115 K). For comparison, v of 1.0–2.9 and Θ of 19–72 are found in SnSe.⁸ The transverse acoustic (TA) branch of BaPdS₂ is particular soft, with $v = 0.5$ km/s (0.8 km/s) and $\Theta = 43$ K (42 K) along the x (z) direction. Animations of the TA phonons along X (featuring rigid PdS₂ chains sliding in the z direction with respect to the others) and along Z (featuring oscillations of the individual PdS₂ chains in the x direction) are included in the Supplemental Material. We note that the behavior of the TA branch is significantly harder along the y direction in terms of the group velocity (1.9 km/s), though not the Debye temperature (49 K). Corresponding to PdS₂ chains sliding in the z direction, the TA branch along Y corresponds to a similar atomic motion to that along X; the significantly larger inter-chain distance in the y direction (10.8 Å) compared to that in x direction (6.9 Å) may be responsible for the very different phonon properties.

Branch	BaPdS ₂				SnSe		
	γ_{all}	$\gamma_{\Gamma X}$	$\gamma_{\Gamma Y}$	$\gamma_{\Gamma Z}$	$\gamma_{\Gamma X}$	$\gamma_{\Gamma Y}$	$\gamma_{\Gamma Z}$
TA	25.5	80.3	0.3	22.8	5.1	2.7	1.0
TA'	2.8	2.6	3.1	1.0	1.1	2.4	2.7
LA	2.3	2.1	1.2	4.0	5.9	1.3	3.3
Avg.	10.2	28.3	1.5	9.3	4.1	2.1	2.3

TABLE II. Averages (computed as $\sqrt{\langle \gamma^2 \rangle}$) of mode Grüneisen parameter $\gamma_{\mathbf{q}\nu}$ for BaPdS₂ and SnSe⁸ for different acoustic branches and directions. For BaPdS₂, the average over the entire high-symmetry path in the Brillouin zone is also given as γ_{all} .

To acquire a baseline assessment for the overall magnitude of the anharmonicity, i.e., the phonon-phonon scattering strength, we compute the mode Grüneisen parameter

$$\gamma_{\mathbf{q}\nu} = -\frac{\partial \omega_{\mathbf{q}\nu} / \omega_{\mathbf{q}\nu}}{\partial V / V}, \quad (2)$$

where V is the volume and $\omega_{\mathbf{q}\nu}$ is the phonon frequency for crystal momentum \mathbf{q} and branch ν . The low-frequency phonons of BaPdS₂, colored by $|\gamma|$, are shown in Fig. 3(b), whereas the full dispersion of $\gamma_{\mathbf{q}\nu}$ for the acoustic branches is included in Fig. 3(c). The most prominent feature is that BaPdS₂ has gigantic $\gamma_{\mathbf{q}\nu}$ for the TA branch along Γ -X (values up to ~ 125) and Γ -Z (values up to ~ 35), which indicates extremely anharmonic interactions for this acoustic branch in BaPdS₂. We perform tests to confirm the large computed $\gamma_{\mathbf{q}\nu}$ are not a numerical artifact, as discussed in the Supplemental Material. Averages of the mode Grüneisen parameter for each acoustic branch of BaPdS₂, averaged over Γ -X, Γ -Y, Γ -Z, and the full high-symmetry path in the Brillouin zone, are shown in Table II, in which we also compare to literature results for SnSe.⁸ The average $\gamma_{\mathbf{q}\nu}$ for the TA branch of BaPdS₂ is 80.3 in the x direction and 22.8 in the z direction, compared to much smaller (less anharmonic) values of 5.1 and 1.0 for SnSe in the

corresponding directions. We note that a key exception to the large anharmonicity of the TA branch of BaPdS₂ is along the y direction, for which the average $\gamma_{\mathbf{q}\nu}$ is only 0.3, as compared to 2.7 for SnSe. In other words, the TA branch of BaPdS₂ is not only harder in the y direction than the other directions, but also much less anharmonic. Although the most remarkable finding is the extremely large $\gamma_{\mathbf{q}\nu}$ for the TA branch, we also find significant anharmonicity for other phonon branches. For example, the TA' (LA) branch exhibits appreciable $\gamma_{\mathbf{q}\nu}$ of 1.0–3.1 (1.2–4.0), as compared to 1.1–2.7 (1.3–5.9) for SnSe. Large anharmonicity is also found in the lowest-frequency optical branch, with mode Grüneisen parameter values as large as ~ 12 , as shown in Fig. 3(b). This branch corresponds to oscillation of the Ba sublattice with respect to the PdS₂ chains in the z direction.

We employ the Debye-Callaway model, an approximate model taking into account normal and Umklapp acoustic phonon-phonon scattering via the mode Grüneisen parameter, as a means to estimate the lattice thermal conductivity of BaPdS₂.^{43–45} We note that the low-frequency optical phonons with large $\gamma_{\mathbf{q}\nu}$, not taken into account in the Debye-Callaway model, may further lower κ_L compared to the values reported here. The contributions of each acoustic phonon branch to κ_L as a function of T in the x , y , and z directions are shown in Fig. 4(a)–4(c), respectively. BaPdS₂ exhibits ultralow lattice thermal conductivity (κ_L less than 1 W/m-K) in the x and z directions. In these directions, the predicted κ_L are of the same magnitude as that of SnSe along its smallest- κ_L direction (values of ~ 0.25 – 0.7 W/m-K).⁸ For BaPdS₂, the main contributor to κ_L in the x direction is the LA branch, which exhibits the largest group velocity; the main contributor in the z direction is the TA' branch, which is the least anharmonic. Like the power factor, the thermal transport is highly anisotropic: in the y direction, κ_L is much larger (values of 4–8 W/m-K) than in the other directions, stemming primarily from the small $\gamma_{\Gamma Y}$ of 0.3 for the TA branch, as discussed above. In the x and z (but not y) directions, BaPdS₂ achieves the minimum possible κ_L , shown as red lines in Fig. 4(a)–4(c), estimated from the model of Cahill *et al.* Overall, BaPdS₂ is predicted to exhibit remarkably poor thermal transport in directions other than y .

As illustrated in Fig. 4(d)–4(f), the combination of large power factor and low κ_L leads to impressive figure of merit for BaPdS₂, particularly in the x direction for electron doping and in the z direction for both electron and hole doping. At high temperature, we find peak ZT values of nearly 3 in the x direction (for 6.0×10^{19} electrons/cm³) and values of nearly 2.3 in the z direction (for 1.1×10^{20} electrons/cm³ or 1.6×10^{20} holes/cm³). In contrast, much smaller peak ZT (< 1) is observed for BaPdS₂ in the y direction, due to the smaller power factor and larger κ_L . In order to obtain the predicted ZT values discussed above, we have chosen an electronic relaxation time (τ) of 5 fs. While an *ab initio* estimation of τ (e.g., from electron-phonon scattering calculations)

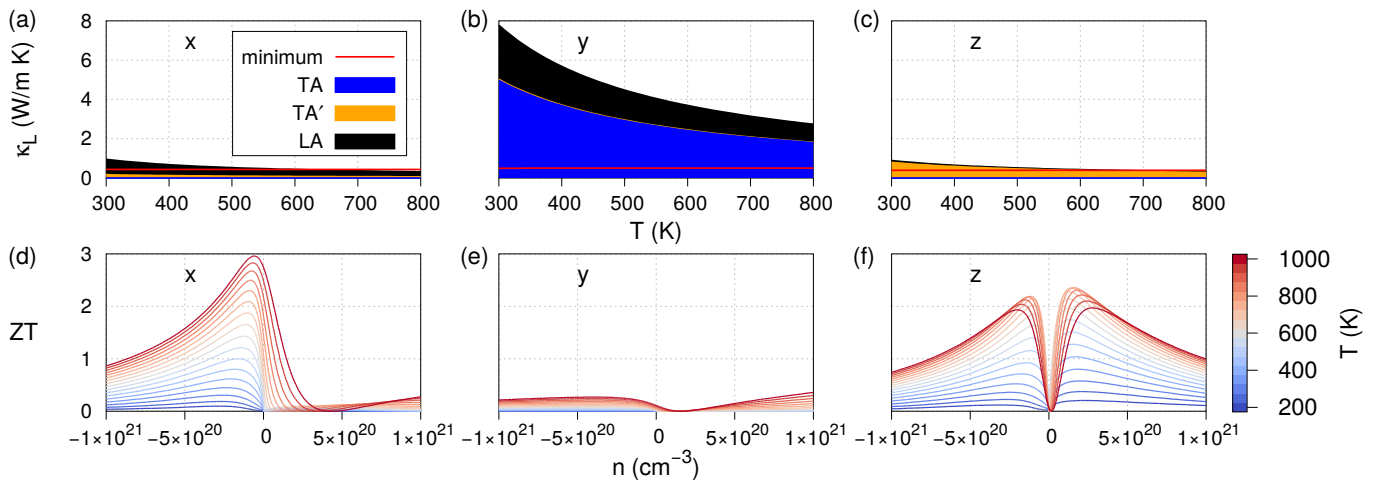


FIG. 4. (a)–(c) Stacked plots of BaPdS₂ acoustic branch contributions to κ_L versus T computed via the Debye-Callaway model for the (a) x , (b) y , and (c) z directions, respectively. Red lines indicate the minimum κ_L of the Cahill model. (d)–(f) ZT as a function of carrier concentration for different T in the (d) x , (e) y , and (f) z directions, respectively. Values are shown for $\tau = 5$ fs.

will be important future work, we note that 5 fs is reasonable in terms of the order of magnitude^{56,57} and can be considered a conservative estimate based on previous works.^{11,24–28} Even with a less optimistic guess for the electronic scattering time, we still find quite large values for the thermoelectric figure of merit, albeit at larger doping. For example, assuming $\tau = 1$ fs, a peak ZT of 1.3 is achieved in the x direction for 2.0×10^{20} electrons/cm 3 . Therefore, even with the uncertainty in τ , our results strongly suggest BaPdS₂ merits experimental investigation.

IV. CONCLUSIONS

BaPdS₂, previously identified by our inverse band structure design approach, is a square planar sulfide material with remarkable, anisotropic thermoelectric properties. Due to a pudding-mold valence band structure and multiple conduction bands, BaPdS₂ exhibits impres-

sive power factor behavior in two of the crystallographic directions. With heavy Ba atoms and extremely soft and anharmonic bonding, BaPdS₂ achieves ultralow lattice thermal conductivity in the x and z directions. We predict peak ZT values of 2–3 in the x direction (n -type) and the z direction (n - and p -type) for an electronic relaxation time of 5 fs. Our results strongly suggest BaPdS₂ warrants experimental investigation for its remarkable electronic, thermal transport, and thermoelectric properties.

ACKNOWLEDGMENTS

We acknowledge support from the U.S. Department of Energy under Contract DE-SC0014520. Computational resources were provided by the National Energy Research Scientific Computing Center (U.S. Department of Energy Contract DE-AC02-05CH11231) and the Extreme Science and Engineering Discovery Environment (National Science Foundation Contract ACI-1548562).

* c-wolverton@northwestern.edu

¹ H. J. Goldsmid, *Introduction to Thermoelectricity*, Springer Series in Materials Science, Vol. 121 (Springer, Berlin, Heidelberg, 2010).

² A. Zevalkink, D. M. Sniadak, J. L. Blackburn, A. J. Ferguson, M. L. Chabinyk, O. Delaire, J. Wang, K. Kovnir, J. Martin, L. T. Schelhas, T. D. Sparks, S. D. Kang, M. T. Dylla, G. J. Snyder, B. R. Ortiz, and E. S. Toberer, *Appl. Phys. Rev.* **5**, 021303 (2018).

³ Y. Pei, H. Wang, and G. J. Snyder, *Adv. Mater.* **24**, 6125 (2012).

⁴ K. Kuroki and R. Arita, *J. Phys. Soc. Jpn.* **76**, 083707 (2007).

⁵ L. D. Hicks and M. S. Dresselhaus, *Phys. Rev. B* **47**, 12727 (1993).

⁶ L. D. Hicks and M. S. Dresselhaus, *Phys. Rev. B* **47**, 16631 (1993).

⁷ H. Usui and K. Kuroki, *J. Appl. Phys.* **121**, 165101 (2017).

⁸ L.-D. Zhao, S.-H. Lo, Y. Zhang, H. Sun, G. Tan, C. Uher, C. Wolverton, V. P. Dravid, and M. G. Kanatzidis, *Nature* **508**, 373 (2014).

⁹ K. Kutorasinski, B. Wiendlocha, S. Kaprzyk, and J. Tobola, *Phys. Rev. B* **91**, 205201 (2015).

¹⁰ Z. Wang, C. Fan, Z. Shen, C. Hua, Q. Hu, F. Sheng, Y. Lu, H. Fang, Z. Qiu, J. Lu, Z. Liu, W. Liu, Y. Huang, Z.-A. Xu, D. W. Shen, and Y. Zheng, *Nat. Commun.* **9**, 47 (2018).

- ¹¹ D. I. Bilc, G. Hautier, D. Waroquiers, G.-M. Rignanese, and P. Ghosez, *Phys. Rev. Lett.* **114**, 136601 (2015).
- ¹² L. K. Lamontagne, G. Laurita, M. W. Gaultois, M. Knight, L. Ghadbeigi, T. D. Sparks, M. E. Gruner, R. Pentcheva, C. M. Brown, and R. Seshadri, *Chem. Mater.* **28**, 3367 (2016).
- ¹³ J. He, S. Hao, Y. Xia, S. S. Naghavi, V. Ozoliņš, and C. Wolverton, *Chem. Mater.* **29**, 2529 (2017).
- ¹⁴ E. B. Isaacs and C. Wolverton, *Chem. Mater.* **30**, 1540 (2018).
- ¹⁵ J. He, Y. Liu, and R. Funahashi, *J. Mater. Res.* **26**, 1762 (2011).
- ¹⁶ K. F. Garrity, *Phys. Rev. B* **94**, 045122 (2016).
- ¹⁷ G. J. Snyder and E. S. Toberer, *Nat. Mater.* **7**, 105 (2008).
- ¹⁸ X. Zhang and L.-D. Zhao, *J. Materiomics* **1**, 92 (2015).
- ¹⁹ G. Tan, L.-D. Zhao, and M. G. Kanatzidis, *Chem. Rev.* **116**, 12123 (2016).
- ²⁰ K. L. Yao, L. Q. Wang, and Z. L. Liu, *Solid State Comm.* **130**, 741 (2004).
- ²¹ R. Bhatt, S. Bhattacharya, R. Basu, A. Singh, U. Deshpande, C. Surger, S. Basu, D. K. Aswal, and S. K. Gupta, *Thin Solid Films* **539**, 41 (2013).
- ²² J. Sun, H. Shi, T. Siegrist, and D. J. Singh, *Appl. Phys. Lett.* **107**, 153902 (2015).
- ²³ J. Huster and W. Bronger, *J. Less Common Met.* **119**, 159 (1986).
- ²⁴ G. K. H. Madsen, *J. Am. Chem. Soc.* **128**, 12140 (2006).
- ²⁵ A. N. Gandi and U. Schwingenschlgl, *Chem. Mater.* **26**, 6628 (2014).
- ²⁶ F. Q. Wang, S. Zhang, J. Yu, and Q. Wang, *Nanoscale* **7**, 15962 (2015).
- ²⁷ S. Hao, F. Shi, V. P. Dravid, M. G. Kanatzidis, and C. Wolverton, *Chem. Mater.* **28**, 3218 (2016).
- ²⁸ K. Pal, J. He, and C. Wolverton, *Chem. Mater.* (2018), 10.1021/acs.chemmater.8b03130.
- ²⁹ P. Hohenberg and W. Kohn, *Phys. Rev.* **136**, B864 (1964).
- ³⁰ W. Kohn and L. J. Sham, *Phys. Rev.* **140**, A1133 (1965).
- ³¹ J. P. Perdew, K. Burke, and M. Ernzerhof, *Phys. Rev. Lett.* **77**, 3865 (1996).
- ³² P. E. Blöchl, *Phys. Rev. B* **50**, 17953 (1994).
- ³³ G. Kresse and D. Joubert, *Phys. Rev. B* **59**, 1758 (1999).
- ³⁴ G. Kresse and J. Hafner, *Phys. Rev. B* **49**, 14251 (1994).
- ³⁵ G. Kresse and J. Hafner, *Phys. Rev. B* **47**, 558 (1993).
- ³⁶ G. Kresse and J. Furthmüller, *Phys. Rev. B* **54**, 11169 (1996).
- ³⁷ G. Kresse and J. Furthmüller, *Comput. Mater. Sci.* **6**, 15 (1996).
- ³⁸ W. Setyawan and S. Curtarolo, *Comput. Mater. Sci.* **49**, 299 (2010).
- ³⁹ G. K. H. Madsen and D. J. Singh, *Comput. Phys. Commun.* **175**, 67 (2006).
- ⁴⁰ A. Togo, F. Oba, and I. Tanaka, *Phys. Rev. B* **78**, 134106 (2008).
- ⁴¹ P. Erhart, B. Sadigh, A. Schleife, and D. Åberg, *Phys. Rev. B* **91**, 165206 (2015).
- ⁴² A. H. Larsen, J. J. Mortensen, J. Blomqvist, I. E. Castelli, R. Christensen, M. Dulak, J. Friis, M. N. Groves, B. Hammer, C. Hargus, E. D. Hermes, P. C. Jennings, P. B. Jensen, J. Kermode, J. R. Kitchin, E. L. Kolsbjerg, J. Kubal, K. Kaasbjerg, S. Lysgaard, J. B. Maronsson, T. Maxson, T. Olsen, L. Pastewka, A. Peterson, C. Rostgaard, J. Schiøtz, O. Schütt, M. Strange, K. S. Thygesen, T. Vegge, L. Vilhelmsen, M. Walter, Z. Zeng, and K. W. Jacobsen, *J. Phys. Condens. Matter* **29**, 273002 (2017).
- ⁴³ J. Callaway, *Phys. Rev.* **113**, 1046 (1959).
- ⁴⁴ D. T. Morelli, J. P. Heremans, and G. A. Slack, *Phys. Rev. B* **66**, 195304 (2002).
- ⁴⁵ Y. Zhang, *J. Materiomics* **2**, 237 (2016).
- ⁴⁶ D. G. Cahill, S. K. Watson, and R. O. Pohl, *Phys. Rev. B* **46**, 6131 (1992).
- ⁴⁷ See Supplemental Material for additional details on electronic and thermal transport methods, phonon and anharmonicity calculation convergence, animations of several low-frequency phonon modes, comparison to experimental crystal structure and formation energy, and the electronic band structure for a different high-symmetry crystal momentum path.
- ⁴⁸ L.-D. Zhao, G. Tan, S. Hao, J. He, Y. Pei, H. Chi, H. Wang, S. Gong, H. Xu, V. P. Dravid, C. Uher, G. J. Snyder, C. Wolverton, and M. G. Kanatzidis, *Science* **351**, 141 (2015).
- ⁴⁹ A. T. Duong, V. Q. Nguyen, G. Duvjir, V. T. Duong, S. Kwon, J. Y. Song, J. K. Lee, J. E. Lee, S. Park, T. Min, J. Lee, J. Kim, and S. Cho, *Nat. Commun.* **7**, 13713 (2016).
- ⁵⁰ C. Chang, M. Wu, D. He, Y. Pei, C.-F. Wu, X. Wu, H. Yu, F. Zhu, K. Wang, Y. Chen, L. Huang, J.-F. Li, J. He, and L.-D. Zhao, *Science* **360**, 778 (2018).
- ⁵¹ Y. Pei, X. Shi, A. LaLonde, H. Wang, L. Chen, and G. J. Snyder, *Nature* **473**, 66 (2011).
- ⁵² W. Liu, X. Tan, K. Yin, H. Liu, X. Tang, J. Shi, Q. Zhang, and C. Uher, *Phys. Rev. Lett.* **108**, 166601 (2012).
- ⁵³ Y. Tang, Z. M. Gibbs, L. A. Agapito, G. Li, H.-S. Kim, M. B. Nardelli, S. Curtarolo, and G. J. Snyder, *Nat. Mater.* **14**, 1223 (2015).
- ⁵⁴ W. G. Zeier, A. Zevalkink, Z. M. Gibbs, G. Hautier, M. G. Kanatzidis, and G. J. Snyder, *Angew. Chem. Int. Ed.* **55**, 6826 (2016).
- ⁵⁵ W. G. Zeier, *Curr. Opin. Green Sustain. Chem.* **4**, 23 (2017).
- ⁵⁶ N. W. Ashcroft and N. D. Mermin, *Solid State Physics* (Saunders College Publishing, 1976).
- ⁵⁷ P. Y. Yu and M. Cardona, *Fundamentals of Semiconductors: Physics and Material Properties* (Springer-Verlag, 1996).